



# IP<sub>3</sub>R-driven increases in mitochondrial Ca<sup>2+</sup> promote neuronal death in NPC disease

Scott A. Tiscione<sup>a</sup>, Maria Casas<sup>a</sup>, Jonathan D. Horvath<sup>a</sup>, Vincent Lam<sup>a</sup>, Keiko Hino<sup>b</sup>, Daniel S. Ory<sup>c</sup>, L. Fernando Santana<sup>a</sup>, Sergi Simó<sup>b</sup>, Rose E. Dixon<sup>a</sup>, and Eamonn J. Dickson<sup>a,1</sup>

<sup>a</sup>Department of Physiology and Membrane Biology, University of California, Davis, CA 95616; <sup>b</sup>Department of Cell Biology and Human Anatomy, University of California, Davis, CA 95616; and <sup>c</sup>Department of Internal Medicine, Washington University School of Medicine, St. Louis, MO 63110

Edited by Mark T. Nelson, University of Vermont, Burlington, VT, and approved July 31, 2021 (received for review June 9, 2021)

**Ca<sup>2+</sup> is the most ubiquitous second messenger in neurons whose spatial and temporal elevations are tightly controlled to initiate and orchestrate diverse intracellular signaling cascades. Numerous neuropathologies result from mutations or alterations in Ca<sup>2+</sup> handling proteins; thus, elucidating molecular pathways that shape Ca<sup>2+</sup> signaling is imperative. Here, we report that loss-of-function, knockout, or neurodegenerative disease-causing mutations in the lysosomal cholesterol transporter, Niemann-Pick Type C1 (NPC1), initiate a damaging signaling cascade that alters the expression and nanoscale distribution of IP<sub>3</sub>R type 1 (IP<sub>3</sub>R1) in endoplasmic reticulum membranes. These alterations detrimentally increase G<sub>q</sub>-protein coupled receptor-stimulated Ca<sup>2+</sup> release and spontaneous IP<sub>3</sub>R1 Ca<sup>2+</sup> activity, leading to mitochondrial Ca<sup>2+</sup> cytotoxicity. Mechanistically, we find that SREBP-dependent increases in Presenilin 1 (PS1) underlie functional and expressional changes in IP<sub>3</sub>R1. Accordingly, expression of PS1 mutants recapitulate, while PS1 knockout abrogates Ca<sup>2+</sup> phenotypes. These data present a signaling axis that links the NPC1 lysosomal cholesterol transporter to the damaging redistribution and activity of IP<sub>3</sub>R1 that precipitates cell death in NPC1 disease and suggests that NPC1 is a nanostructural disease.**

calcium | IP<sub>3</sub>R | NPC1 | neurodegeneration | GPCR

Calcium (Ca<sup>2+</sup>) is the most-ubiquitous second messenger in neurons. For this reason, spatial and temporal elevations in cytosolic Ca<sup>2+</sup> signals are tightly controlled, with elevations in cytoplasmic Ca<sup>2+</sup> used to initiate and orchestrate a host of diverse intracellular signaling cascades fundamentally required for neuronal development, synaptic plasticity, neurotransmission, and neuron fidelity (for review, refer to refs. 1, 2). One of the primary mechanisms to elevate intracellular Ca<sup>2+</sup> levels is through release of Ca<sup>2+</sup> from the largest intracellular Ca<sup>2+</sup> store, the endoplasmic reticulum (ER). Ca<sup>2+</sup> can be rapidly mobilized from the ER into the cytoplasm through the Inositol 1,4,5-triphosphate receptor (IP<sub>3</sub>R), a ligand-gated Ca<sup>2+</sup> channel in the ER membrane. IP<sub>3</sub>Rs are activated when cell surface G<sub>q</sub>-protein coupled receptors (G<sub>q</sub>PCR) stimulate phospholipase C (PLC) to hydrolyze the plasma membrane (PM) lipid PI(4,5)P<sub>2</sub> into soluble IP<sub>3</sub>, the native agonist of the IP<sub>3</sub>Rs (3). IP<sub>3</sub>Rs are further regulated by phosphorylation, protein-protein interactions, and local Ca<sup>2+</sup> concentrations (3, 4).

Niemann-Pick Type C1 (NPC1) disease is an autosomal recessive lysosomal storage disorder that arises from mutations in the gene encoding the lysosomal NPC1 protein. This transmembrane cholesterol transporter facilitates the egress of cholesterol from the acidic compartment to other cellular membranes with its loss-of-function resulting in the cellular hallmark of NPC1 disease: an accumulation of lipids within the lysosome and perturbations in cellular cholesterol homeostasis. The underlying mechanisms linking cholesterol dysregulation and lipid accumulation to neurodegeneration are not well understood; however, impaired Ca<sup>2+</sup> signaling is a consequence of NPC1 disease mutations (5–7). Given that dysfunctional Ca<sup>2+</sup> signaling is a common feature in neurodegenerative disease and is thought to precede and contribute to neuronal cell death (2, 8), understanding the link between NPC1 function and intracellular Ca<sup>2+</sup> becomes imperative.

There are three IP<sub>3</sub>R isoforms: IP<sub>3</sub>R Type 1 (IP<sub>3</sub>R1), Type 2, and Type 3, each with its own differential expression across cell types and tissues. IP<sub>3</sub>R1 protein is most abundantly expressed in soma and synaptic regions of the brain, including Purkinje cells of the cerebellum (9), the most impacted cell type in NPC1 disease (10). Functionally, IP<sub>3</sub>R1 is essential for a variety of intracellular events including G<sub>q</sub>PCR signaling (11), synaptic strengthening (12), Ca<sup>2+</sup>-dependent gene transcription (11), and Ca<sup>2+</sup> transfer at ER-mitochondrial membrane contact sites (MCS) (13). Behaviorally, IP<sub>3</sub>R1<sup>-/-</sup> mice die in utero or only live for a few weeks while exhibiting severe neurological symptoms such as ataxia and seizures (14), while specific cerebellum loss (15) or disease mutations in the IP<sub>3</sub>R1 gene lead to ataxias (16, 17) and Gillespie syndrome (18). Given IP<sub>3</sub>R1's importance in neurological function and development, and our previous reports of decreased PI(4,5)P<sub>2</sub> levels (precursor of IP<sub>3</sub>) as well as reductions in ER Ca<sup>2+</sup> (source of G<sub>q</sub>PCR Ca<sup>2+</sup>) in multiple models of NPC disease (19, 20), we hypothesized that IP<sub>3</sub>R signaling may be perturbed in NPC1 disease.

Using a combination of murine and patient disease models of NPC1 disease, we show that despite reduced PI(4,5)P<sub>2</sub> (19) and ER Ca<sup>2+</sup> (20), IP<sub>3</sub>-mediated Ca<sup>2+</sup> release is paradoxically increased. We determine that loss of NPC1 function results in larger and more numerous immobile IP<sub>3</sub>Rs clusters near the PM that drive spontaneous Ca<sup>2+</sup> release events (Ca<sup>2+</sup> puffs) and prime IP<sub>3</sub>R to release more Ca<sup>2+</sup> during G<sub>q</sub>PCR activation. The cellular consequences of enhanced IP<sub>3</sub>R clustering and activity are 1) decreased ER Ca<sup>2+</sup> levels, 2) increased nuclear factor of activated T-cells (NFAT) signaling, and 3) increased mitochondrial

## Significance

**NPC1 is a ubiquitously expressed lysosomal cholesterol transporter whose loss of function results in neurodegenerative NPC1 disease. Here, we report that loss-of-function, knockout, or mutation-causing NPC1 initiates a damaging signaling cascade that alters the expression and nanoscale distribution of IP<sub>3</sub>R type 1 that precipitates neuron death. Targeting IP<sub>3</sub>R1 or upstream elements of this signaling cascade rescues neuronal death and provides potential therapeutic targets to address IP<sub>3</sub>R dysfunction, a feature of NPC1 disease and other neurodegenerative disorders.**

Author contributions: S.A.T., M.C., R.E.D., and E.J.D. designed research; S.A.T., M.C., J.D.H., V.L., K.H., S.S., and E.J.D. performed research; D.S.O. and L.F.S. contributed new reagents/analytic tools; S.A.T., M.C., J.D.H., V.L., K.H., S.S., R.E.D., and E.J.D. analyzed data; and S.A.T., M.C., J.D.H., D.S.O., L.F.S., S.S., R.E.D., and E.J.D. wrote the paper.

The authors declare no competing interest.

This article is a PNAS Direct Submission.

This open access article is distributed under [Creative Commons Attribution-NonCommercial-NoDerivatives License 4.0 \(CC BY-NC-ND\)](https://creativecommons.org/licenses/by-nc-nd/4.0/).

<sup>1</sup>To whom correspondence may be addressed. Email: ejdickson@ucdavis.edu.

This article contains supporting information online at <https://www.pnas.org/lookup/suppl/doi:10.1073/pnas.2110629118/-DCSupplemental>.

Published September 27, 2021.

Ca<sup>2+</sup>, which leads to neuronal Ca<sup>2+</sup> cytotoxicity. We propose that the lysosomal NPC1 cholesterol transporter can tune the distribution and activity of IP<sub>3</sub>R in health, while its loss of function, such as in NPC1 disease, initiates a pervasive signaling cascade that triggers mitochondrial cytotoxicity.

## Results

**Loss of NPC1 Function Potentiates G<sub>q</sub>-Mediated Ca<sup>2+</sup> Signaling.** We have previously reported that both ER-Ca<sup>2+</sup> stores and PM PI(4,5)P<sub>2</sub> levels are significantly reduced in NPC1 disease (19, 20). Given that IP<sub>3</sub>R-mediated Ca<sup>2+</sup> release requires both a steep Ca<sup>2+</sup> gradient across the ER and IP<sub>3</sub>'s precursor, PI(4,5)P<sub>2</sub>; (Fig. 1A), we tested the hypothesis that cytosolic Ca<sup>2+</sup> signals evoked from IP<sub>3</sub>R following activation of a G<sub>q</sub>PCR were perturbed in NPC1 loss-of-function cells. First, we compared G<sub>q</sub>PCR responses from control and U18666A-treated (U18; specific inhibitor of NPC1) (21) tsA201 cells loaded with the cytosolic Ca<sup>2+</sup> indicator Fluo-4 and treated with histamine, an agonist for the G<sub>q</sub>-coupled histamine H<sub>1</sub> receptor, in a Ca<sup>2+</sup>-free solution to eliminate extracellular Ca<sup>2+</sup> contribution. Analysis of the resulting Ca<sup>2+</sup> responses revealed that overnight inhibition of NPC1 significantly increased the amount of Ca<sup>2+</sup> released into the cytoplasm (Fig. 1B and C). Similar results were observed from NPC1<sup>-/-</sup> cells (Fig. 1D and E) and patient fibroblasts harboring the most prevalent patient mutation (NPC1<sup>I1061T</sup>; Fig. 1F and G). To confirm that NPC1-dependent increases in G<sub>q</sub>PCR-mediated Ca<sup>2+</sup> release were conserved in neurons, we performed similar experiments in two murine models of NPC1 disease: 1) NPC1 knockout (NPC1<sup>-/-</sup>) neurons and 2) Npc1<sup>tm(I1061T)Dso</sup> (hereafter referred to as NPC1<sup>I1061T</sup>) neurons, which recapitulate the pathological features of the most prevalent human disease allele (22). Similar to cell models, both NPC1<sup>-/-</sup> (Fig. 1H and I) and NPC1<sup>I1061T</sup> (Fig. 1J and K) neurons exhibited significantly larger elevations

in Ca<sup>2+</sup> following G<sub>q</sub>PCR stimulation as compared to wild type (WT) control neurons. Thus, across all models of NPC1 disease, including primary neurons, IP<sub>3</sub>R-mediated Ca<sup>2+</sup> release was significantly increased.

**NPC1 Inhibition or Disease Mutation Alters IP<sub>3</sub>R1 Expression and Distribution.** To determine the molecular mechanism(s) underlying increased G<sub>q</sub>PCR-induced Ca<sup>2+</sup> release, we first measured mRNA levels from each of the PM elements along the G<sub>q</sub>PCR signaling cascade from receptors to PLC enzymes (SI Appendix, Fig. S1A and B). Quantification of gene transcripts from control and NPC1<sup>I1061T</sup> patient cells revealed that several varieties of receptor, Gα<sub>q</sub>, and PLC isoforms were unaltered following loss of NPC1 function. The sole exception was PLCβ2, which had elevated messenger ribonucleic acid (mRNA) levels (SI Appendix, Fig. S1B) but unaltered protein levels (SI Appendix, Fig. S1C) in NPC1<sup>I1061T</sup> cells relative to control. Based on these analyses, the observation that three different G<sub>q</sub>PCR agonists (histamine, purinergic, and muscarinic) all resulted in enhanced Ca<sup>2+</sup> release (Fig. 1B–K), and our previous determination that PM PI(4,5)P<sub>2</sub> is decreased in NPC1 disease (19) suggest that the molecular element(s) responsible for enhancing G<sub>q</sub>PCR signaling in NPC1 disease cells do not lie at the PM.

We next examined whether elements downstream of PI(4,5)P<sub>2</sub> are involved in potentiating G<sub>q</sub>PCR Ca<sup>2+</sup> release in NPC1 cells. To begin, we analyzed IP<sub>3</sub>R1, as it is 1) the most common isoform in the brain and 2) abundantly expressed in Purkinje cells of the cerebellum (9), the most vulnerable neuronal cell type in NPC (23). Western blot analysis determined that NPC1<sup>I1061T</sup> patient cells had a 2.6-fold increase in protein levels compared to control (Fig. 2A). To test whether this expressional change in IP<sub>3</sub>R1 protein levels translates to a functional role in potentiating G<sub>q</sub>PCR Ca<sup>2+</sup> release, we treated IP<sub>3</sub>R1 knockout (IP<sub>3</sub>R1<sup>-/-</sup>) human embryonic

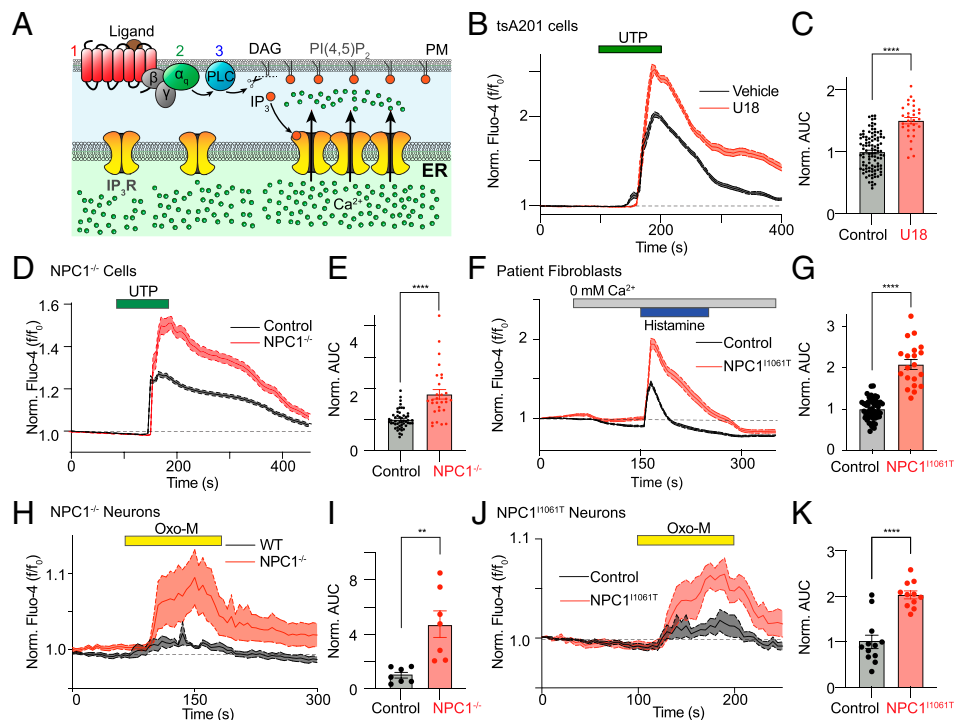


**Fig. 1.** G<sub>q</sub>PCR Ca<sup>2+</sup> release is enhanced in NPC1 disease. (A) G<sub>q</sub>PCR signaling pathway. (B) Average time series of Fluo-4 loaded control (black) and U18-treated (red) tsA201 cells treated with UTP (100 μM). (C) Quantitative analysis of the UTP-evoked Ca<sup>2+</sup> area under the curve (AUC). (D and E) Same as B and C, only NPC1<sup>-/-</sup> cells. (F and G) Same as B and C, only control and NPC1<sup>I1061T</sup> patient cells and treated with histamine (100 μM). (H and I) Same as B and C, only NPC1<sup>-/-</sup> neurons treated with Oxo-M. (J and K). Same as B and C, only NPC1<sup>I1061T</sup> neurons treated Oxo-M. All the data are expressed as mean ± SEM from individual cells. Statistical analysis was an unpaired *t* test. \*\*\*\**P* < 0.0001; \*\*\**P* < 0.001; \*\**P* < 0.01.

kidney 293 (HEK) cells with U18 and evoked IP<sub>3</sub>R-mediated Ca<sup>2+</sup> release using the purinergic receptor agonist, UTP (100 μM) (24). Unlike overnight U18 treatment in control cells (Fig. 1*B*), we found that incubating IP<sub>3</sub>R1<sup>-/-</sup> cells with U18 did not alter G<sub>q</sub>PCR Ca<sup>2+</sup> responses (Fig. 2*B* and *C*). These data support a model wherein increased IP<sub>3</sub>R1 protein levels facilitate augmented IP<sub>3</sub>R-mediated signaling following NPC1 dysfunction.

The spatial distribution of IP<sub>3</sub>Rs influences ER Ca<sup>2+</sup> release, inactivation, wave propagation, and oscillations (3, 25–27). To determine whether increased protein levels alter the spatial organization of IP<sub>3</sub>R1, we took several complementary fluorescent approaches to visualize the endogenous distribution of IP<sub>3</sub>R1 in isolated cells, including neurons, and intact brain slices. To begin, we used HeLa cells with endogenous IP<sub>3</sub>R1 tagged with a monomeric eGFP (eGFP-IP<sub>3</sub>R cells) (28). eGFP-IP<sub>3</sub>R cells allow us to quantify the endogenous distribution of the IP<sub>3</sub>R1 without influence from overexpression or off-target binding of immunofluorescent antibodies. Total internal reflection fluorescence (TIRF) microscopy, to visualize IP<sub>3</sub>R1 close to the PM, revealed that U18 treatment increased both the area and number of IP<sub>3</sub>R1 clusters close to the PM (Fig. 2*D* and *E*). To independently confirm that loss of NPC1 function alters IP<sub>3</sub>R1 distribution near the PM, we performed immunofluorescence experiments on patient fibroblasts, neurons, and brain slices from the NPC1<sup>11061T</sup> murine model using a validated IP<sub>3</sub>R1 antibody (SI Appendix, Fig. S2*A–D*). TIRF imaging from patient fibroblasts determined that NPC1 disease mutations also increase IP<sub>3</sub>R1 cluster size and number (Fig. 2*F* and *G*). Similarly, IP<sub>3</sub>R1 cluster intensity and area was increased at both the soma and neurites of isolated hippocampal (Fig. 2*H* and *I*) and cortical neurons (Fig. 2*J* and *K*). Finally, to ensure that 1) IP<sub>3</sub>R1 clustering occurs in intact brain regions and 2) increased IP<sub>3</sub>R1 cluster size occurs in brain regions affected by NPC1 disease, cerebellar slices from age-matched wild-type and symptomatic NPC1<sup>11061T</sup> animals were fixed and double immunostained for IP<sub>3</sub>R1 and the Purkinje cell marker calbindin. In agreement with our single-cell data, IP<sub>3</sub>R1 clusters within the Purkinje cell soma was significantly larger in NPC1 disease cerebellar sections than controls (Fig. 2*L*). Collectively, these data present strong evidence that loss of NPC1 function increases expression and distribution of IP<sub>3</sub>R1 to enhance cluster size and increase G<sub>q</sub>PCR-mediated Ca<sup>2+</sup> release.

**Nanoscale Distribution of IP<sub>3</sub>R1 Is Altered in NPC1 Disease.** Having demonstrated that IP<sub>3</sub>R1 clustering and distribution is altered near the PM in NPC1 disease using diffraction-limited approaches, we next wanted to precisely map and quantify the nanoscale organization of IP<sub>3</sub>R1 at the PM using superresolution single-molecule localization microscopy in TIRF mode (superresolution-TIRF; resolution is approximately 20 nm) (29). This is important, because it allows us to investigate the nanoscale molecular architecture within and between IP<sub>3</sub>R1 clusters to determine whether they are altered in NPC1 disease cells.

Quantitative analysis of superresolution-TIRF localization maps from control and U18-treated eGFP-IP<sub>3</sub>R cells revealed that similar to diffraction-limited images, NPC1 inhibition resulted in an increase in both IP<sub>3</sub>R cluster size and density (Fig. 3*A* and *B*). Similar results were also obtained from neurons (Fig. 3*C* and *D*). During analysis of localization maps, we noticed that single IP<sub>3</sub>R1 clusters visualized using conventional TIRF microscopy actually consisted of many discrete puncta when imaged with superresolution microscopy (SI Appendix, Fig. S3*A–E*). Cells lacking NPC1 function displayed a higher density of puncta in these discrete localized areas (SI Appendix, Fig. S3*D–F*). Further, nearest-neighbor analysis measuring the distance from both a centroid and perimeter (SI Appendix, Fig. S3*C*) of these discrete puncta indicated that puncta were more closely associated with one another in U18-treated cells (SI Appendix, Fig. S3*G–J*). Together, these data present evidence that loss of NPC1 function not only increases

IP<sub>3</sub>R puncta size but also increases the density of IP<sub>3</sub>R1 puncta both within and between a cluster in NPC1 disease.

### IP<sub>3</sub>R1 Cluster Mobility and Activity Are Increased in NPC1 Disease.

Given that IP<sub>3</sub>R1 cluster size is increased in NPC1 disease, we wanted to determine whether the mobility of IP<sub>3</sub>R1 in the ER was altered. To this end, we used fluorescent recovery after photobleaching to quantify the mobility of eGFP-tagged IP<sub>3</sub>R1 clusters both near the PM (SI Appendix, Fig. S4*A–C*) and within the cell interior (SI Appendix, Fig. S4*D–F*). Fitting of fluorescence recovery kinetics after photobleaching revealed that the mobile fraction of IP<sub>3</sub>R1 in U18-treated eGFP-IP<sub>3</sub>R cells was significantly reduced compared to vehicle controls both near the PM (SI Appendix, Fig. S4*C*) and near the middle of the cell (SI Appendix, Fig. S4*F*).

Recently, it has been reported that immobile IP<sub>3</sub>R1 clusters localized close to ER–PM junctions are optimally positioned to respond to receptor-generated IP<sub>3</sub> to initiate Ca<sup>2+</sup> signals (28). Further, immobile IP<sub>3</sub>R clusters have been observed to be the site of spontaneous localized Ca<sup>2+</sup> release from the ER, termed “Ca<sup>2+</sup> puffs” (28), with the activity of puffs further influenced by the number of IP<sub>3</sub>R within the originating cluster (25, 30). Given that IP<sub>3</sub>R1 clusters are larger, contain more discrete IP<sub>3</sub>R1 puncta within a cluster, and are more immobile following NPC1 dysfunction, we wanted to determine whether spontaneous Ca<sup>2+</sup> puffs were altered. First, we loaded eGFP-IP<sub>3</sub>R cells with the Ca<sup>2+</sup> dye Calbryte590 and simultaneously measured IP<sub>3</sub>R1 distribution and spontaneous Ca<sup>2+</sup> activity. This approach allows us to measure and correlate Ca<sup>2+</sup> activity in the same region as IP<sub>3</sub>R1 (Fig. 4*A*). We define this signal simply as Ca<sup>2+</sup><sub>IP<sub>3</sub>R1</sub>, because 1) the Ca<sup>2+</sup> signal originates within the same location as IP<sub>3</sub>R1, 2) is sensitive to the IP<sub>3</sub>R antagonist Xestospongin C (SI Appendix, Fig. S5*A* and *C*), and 3) spontaneous Ca<sup>2+</sup> signals occur in the absence of extracellular Ca<sup>2+</sup> (SI Appendix, Fig. S5*B*). We do acknowledge the possibility that these Ca<sup>2+</sup> signals may not only result from IP<sub>3</sub>R1 but represent a convolved signal from other Ca<sup>2+</sup> sources. That being said, analysis of spontaneous Ca<sup>2+</sup><sub>IP<sub>3</sub>R1</sub> signals determined that the amplitude, duration, and number of spontaneous Ca<sup>2+</sup> events were all significantly elevated in U18-treated cells relative to control (Fig. 4*B* and *C*), consisted with previous reports of increased spontaneous activity with larger IP<sub>3</sub>R clusters.

To test whether disease mutations exhibit altered Ca<sup>2+</sup><sub>IP<sub>3</sub>R1</sub>, we loaded control and NPC1<sup>11061T</sup> patient fibroblasts with Fluo-4 and measured spontaneous Ca<sup>2+</sup> activity. Similar to U18-treated cells, NPC1<sup>11061T</sup> cells also had increased amplitude, duration, and mass (volume) of Ca<sup>2+</sup> puffs compared to healthy controls (Fig. 4*D–I*). To further investigate a role for IP<sub>3</sub>R1 in facilitating these increases in Ca<sup>2+</sup> activity, we treated control and IP<sub>3</sub>R1<sup>-/-</sup> cells with U18 or vehicle control and quantified spontaneous Ca<sup>2+</sup> events. We found that treatment with U18 recapitulated the Ca<sup>2+</sup> puff phenotype observed in eGFP-IP<sub>3</sub>R cells and NPC1<sup>11061T</sup> fibroblasts, while IP<sub>3</sub>R1<sup>-/-</sup> cells were insensitive to the U18 (Fig. 4*J* and *K*). Peak fluorescence of Ca<sup>2+</sup> puffs was also quantified showing no significant difference between vehicle and U18 treatment in both cell types but a significant reduction in IP<sub>3</sub>R1<sup>-/-</sup> cells (Fig. 4*L*). These results indicate that the altered nanoscale distribution of IP<sub>3</sub>R1 contribute to enhanced Ca<sup>2+</sup> puff activity in NPC1 disease.

### Presenilin 1 Alters IP<sub>3</sub>R1 Distribution and Function in NPC1 Disease.

Having established that G<sub>q</sub>PCR-mediated Ca<sup>2+</sup> signaling, IP<sub>3</sub>R1 distribution, and IP<sub>3</sub>R1 activity are all severely altered in NPC1 disease, we next wanted to identify the underlying mechanism(s) responsible for these changes. Recently, we have reported that increases in full-length, holoprotein, Presenilin 1 (PS1) expression is involved in mediating decreases in ER Ca<sup>2+</sup> in NPC1 disease (20). Further, Alzheimer’s disease mutations in PS1 (PS1<sup>D257A</sup>) that shift expression mostly to the holoprotein form have previously been

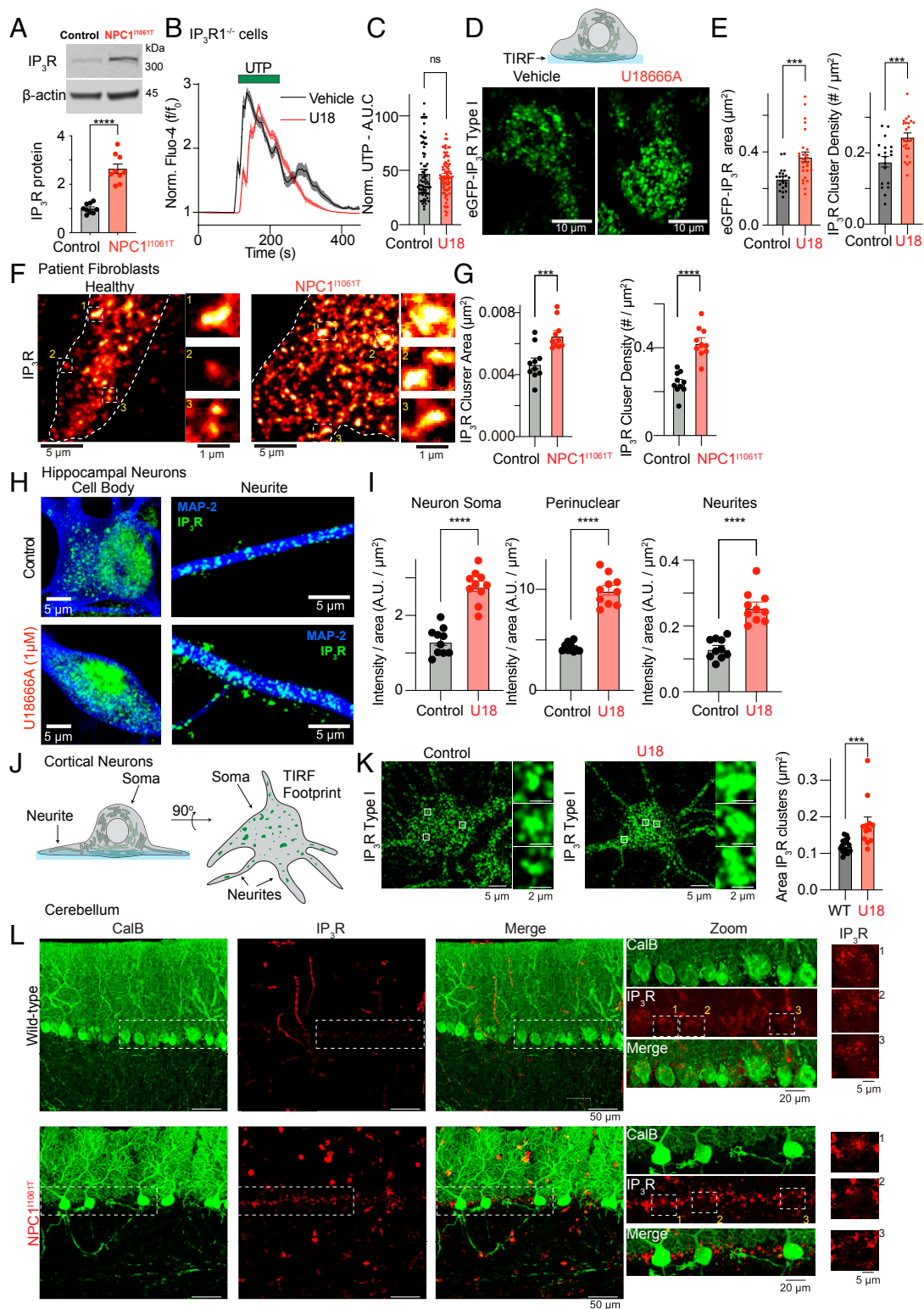


**Fig. 2.** IP<sub>3</sub>R1 expression and distribution is remodeled in NPC1 disease. (A, Top) representative Western blot of IP<sub>3</sub>R1 in control and NPC1<sup>11061T</sup> disease fibroblasts. (Bottom) Quantification of IP<sub>3</sub>R1 protein expression, normalized to β-Actin. (B) Average time series of Fluo-4 loaded control (black) and IP<sub>3</sub>R1<sup>-/-</sup> (red) HEK cells, treated with UTP. (C) Quantitative analysis of the UTP-evoked Ca<sup>2+</sup> area under the curve (AUC). (D, Top) Schematic of TIRF imaging. (Bottom) Representative TIRF images from eGFP-IP<sub>3</sub>R HeLa cells, treated with vehicle (Left) or U18 (Right). (E, Left) Quantification of average IP<sub>3</sub>R puncta area. (Right) IP<sub>3</sub>R density. (F) Representative TIRF images from control (Left) and NPC1<sup>11061T</sup> (Right) patient fibroblasts fixed and stained for IP<sub>3</sub>R1. (G) Quantification of IP<sub>3</sub>R1 cluster area (Left) and density (Right) from patient fibroblasts. (H) Representative images from cell body (Left) and neurite (Right) regions of control (Top) and U18-treated (Bottom) hippocampal neurons fixed and stained for IP<sub>3</sub>R and MAP2. (I) Quantification of IP<sub>3</sub>R intensity. (J) Schematic of TIRF image in neuron. (K) Representative images from control (Left) and U18-treated (Right) cortical neurons fixed and stained for IP<sub>3</sub>R. Insets show zoomed regions containing IP<sub>3</sub>R1 clusters. (Right) Quantification of IP<sub>3</sub>R1 cluster area. (L) Representative cerebellar sections from wild-type (Top) and NPC1<sup>11061T</sup> brains fixed and stained for calbindin and IP<sub>3</sub>R1. All the data are expressed as mean ± SEM from individual cells. Statistical analyses were unpaired t tests. ns: not significant; \*\*\*P < 0.001; \*\*\*\*P < 0.0001.

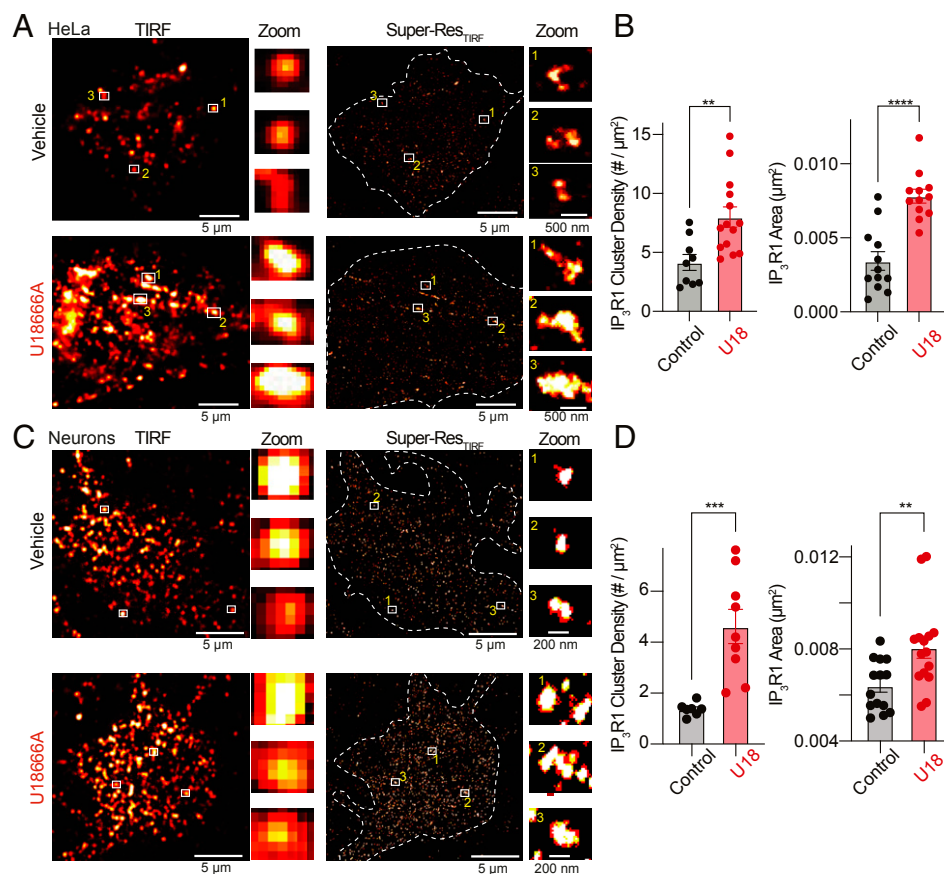


**Fig. 3.** Nanoscale distribution of IP<sub>3</sub>R1 is remodeled in NPC1 disease. (A, Left) Representative TIRF images of Vehicle (Top) and U18-treated (Bottom) eGFP-IP<sub>3</sub>R HeLa cells fixed and immunostained with an anti-GFP antibody. (Right) Superresolution localization map from the same cell. Zoomed regions are from white solid rectangles. (B) Quantification of density and area of eGFP-IP<sub>3</sub>R1. (C and D) Same as A and B, only cortical neurons fixed and stained for IP<sub>3</sub>R1. All the data are expressed as mean ± SEM from individual cells. Statistical analyses were unpaired t tests. \**P* < 0.05; \*\**P* < 0.01; \*\*\**P* < 0.001; \*\*\*\**P* < 0.0001.

reported to interact and produce exaggerated gain of function alterations to the biophysical gating properties of IP<sub>3</sub>Rs (31, 32). To interrogate a role for PS1 in tuning IP<sub>3</sub>R1 distribution/function, we first transfected HeLa cells with HA-PS1 (HA-PS1-WT) or HA-tagged PS1<sup>D257A</sup> and treated overnight with either vehicle control or U18 (10 μM; Fig. 5A and B). TIRF imaging revealed that PS1-WT formed discrete clusters close to the PM, with cluster area significantly increased following overnight treatment with U18 to inhibit NPC1 function (Fig. 5A and B). Interestingly, the PS1<sup>D257A</sup> mutation also clustered close to the PM and displayed a similar mean cluster size as the PS1-WT group treated with U18 (Fig. 5A and B). Treatment of PS1<sup>D257A</sup>-expressing cells with U18 did not further increase PS1 cluster area (Fig. 5B). These data suggest that loss of NPC1 function or Alzheimer's disease mutations increase the size of PS1 clusters near the PM. To test whether these increases correlate with changes in IP<sub>3</sub>R1 distribution, we expressed the aforementioned constructs in eGFP-IP<sub>3</sub>R1 HeLa cells and calculated Pearson's correlation coefficients. Image analysis revealed that U18 treatment significantly increases the colocalization of PS1 to IP<sub>3</sub>R1 (compare Fig. 5C and D), while the PS1<sup>D257A</sup> mutant also colocalizes more with IP<sub>3</sub>R compared to wild-type PS1 even in the absence of NPC1 inhibition (Fig. 5E; analysis in Fig. 5F). These data are consistent with published observations that PS1 physically interacts with IP<sub>3</sub>R1 and suggests there is a strong correlation between PS1 cluster size and IP<sub>3</sub>R1 distribution. To test whether the full-length form of PS1, which is increased in NPC1 disease (20), alters IP<sub>3</sub>R1, we overexpressed PS1<sup>D257A</sup> in eGFP-IP<sub>3</sub>R1 HeLa cells. Aligned with a key role for the holoprotein in mediating the distribution/

function of IP<sub>3</sub>R1, expression of PS1<sup>D257A</sup> increased both IP<sub>3</sub>R1 clusters (Fig. 5G and H) and G<sub>q</sub>PCR-mediated Ca<sup>2+</sup> release (Fig. 5I and J) to a similar extent as disease mutations or inhibition of NPC1. Altogether, these results suggest that enhanced PS1 cluster size may be responsible for altered nanoscale distribution/function of IP<sub>3</sub>R1 following NPC1 loss of function.

A key question remained whether Ca<sup>2+</sup> potentially coming through PS1 (33) can contribute to increases in IP<sub>3</sub>R1, or whether only physical interactions (31) between the two proteins are important. To begin answering this question, we treated eGFP-IP<sub>3</sub>R1 cells with the Sacro/ER Ca<sup>2+</sup>-ATPase (SERCA) inhibitor Thapsigargin or the Ca<sup>2+</sup> chelating agent EGTA in a 0-mM, Ca<sup>2+</sup>-containing extracellular solution (SI Appendix, Fig. S6A–D) and quantified IP<sub>3</sub>R1 clusters near the PM over a period of 60 mins. Under each of these cytoplasmic Ca<sup>2+</sup>-altering conditions, IP<sub>3</sub>R1 cluster size significantly decreased near the PM, independently of alterations in the cell footprint (SI Appendix, Fig. S6E–M). Thus, although modulating cytoplasmic Ca<sup>2+</sup> concentrations does alter IP<sub>3</sub>R1 clustering near the PM, it is in the opposing direction compared to loss of NPC1 function.

Next, to test a direct role for PS1 driving IP<sub>3</sub>R1 alterations in NPC1 disease, we knocked-down or knocked-out PS1 in different cells and measured IP<sub>3</sub>R1 distribution, activity, and G<sub>q</sub>PCR-mediated Ca<sup>2+</sup> release. First, using small interfering RNA (siRNA) directed against PS1 in eGFP-IP<sub>3</sub>R1 HeLa cells, which decreases PS1 protein levels by 75% (20), we determined that IP<sub>3</sub>R1 cluster areas were refractory to U18 treatment (Fig. 6A and B). Second, aligned with its ability to normalize IP<sub>3</sub>R1 clusters back to control sizes, PS1 knock-down in NPC1<sup>I1061T</sup> patient cells

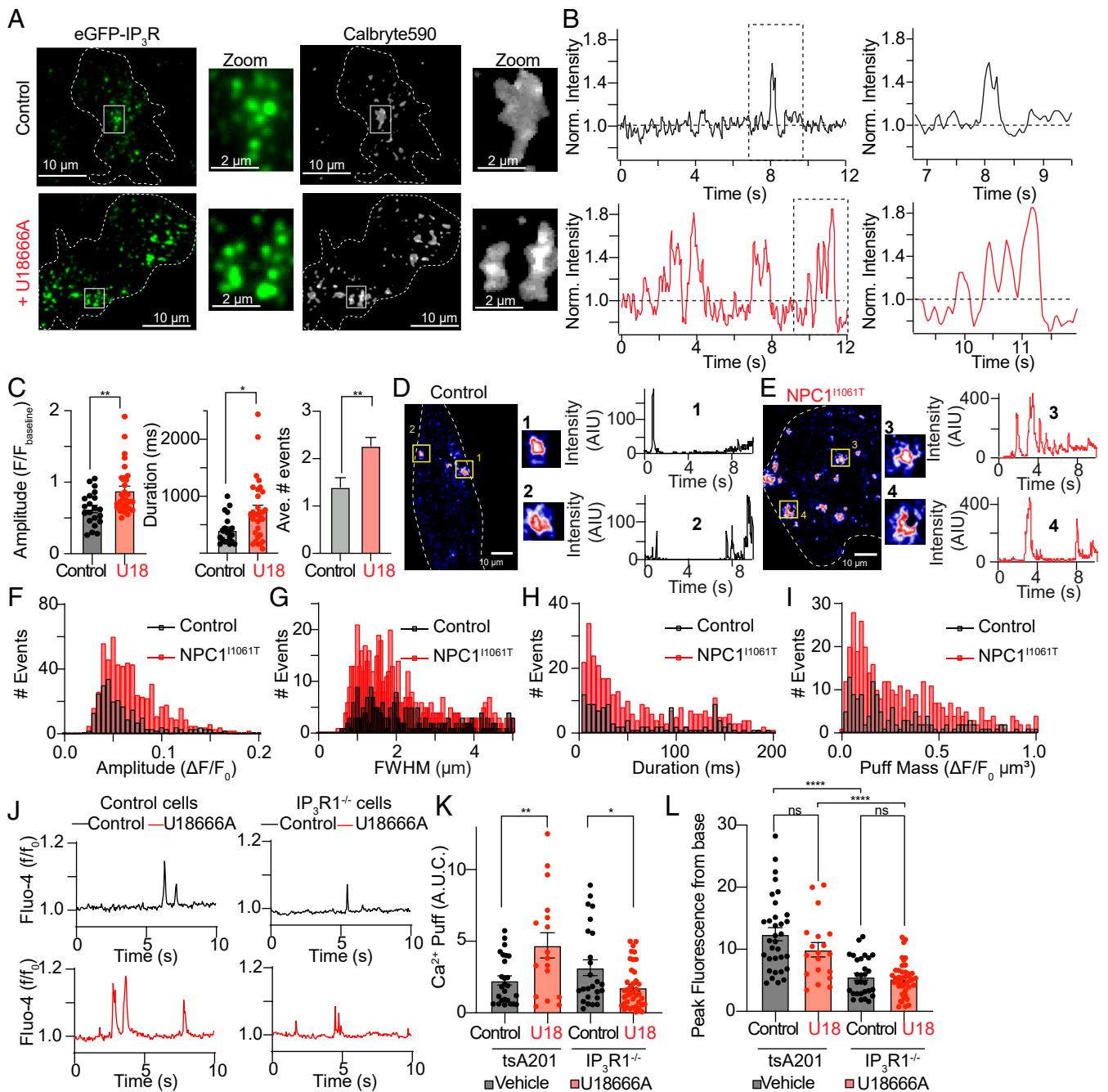


**Fig. 4.** Spontaneous intracellular  $IP_3R1$   $Ca^{2+}$  signaling is enhanced in NPC loss-of-function cells. (A) Representative maximum intensity projections of eGFP- $IP_3R1$  (Left) and Calbryte590 (Right) from control (Top) and U18-treated cells. Zoomed regions are taken from white rectangles. (B) Representative time series of spontaneous  $Ca^{2+}$  puffs in control cells (Top) and U18-treated (Bottom, red lines) cells. (Right) Zoomed time regions taken from dashed black rectangle. (C) Quantification of amplitude, duration, and number of spontaneous  $Ca^{2+}$  events. (D, Left) Representative maximum intensity projections from control fibroblasts loaded with Fluo-4. Zoomed regions are taken from solid yellow squares. (Right) Representative time series of spontaneous  $Ca^{2+}$  activity. (E) Same as D, only NPC1<sup>11061T</sup> patient fibroblasts. (F) Frequency distribution of the amplitude of  $Ca^{2+}$  events from healthy fibroblasts (black) and NPC1<sup>11061T</sup> disease fibroblasts (red). (G) Same as F, except showing the full-width half-max. (H) Same as F, except showing the duration of  $Ca^{2+}$  events. (I) Same as F, except showing  $Ca^{2+}$  puff mass. (J) Representative time series of  $Ca^{2+}$  events in control cells (Left) or  $IP_3R1^{-/-}$  cells (Right) loaded with Fluo-4 and treated with either U18 (red) or vehicle control (black). (K) Quantitative analysis of  $Ca^{2+}$  puff area under the curve from the cell types and conditions in J. (L) Same as K, except analyzing  $Ca^{2+}$  puff peak fluorescence from base. All the data are expressed as mean  $\pm$  SEM from individual cells. Statistical analyses were unpaired t tests except K and L which were two-way ANOVAs. ns: not significant; \* $P < 0.05$ ; \*\* $P < 0.01$ ; \*\*\*\* $P < 0.0001$ .

significantly reduced spontaneous  $Ca^{2+}_{IP_3R1}$  puffs back to control levels (Fig. 6C). Third, NPC1<sup>11061T</sup> patient cells treated with siRNA PS1 had similar  $G_q$ PCR-mediated  $Ca^{2+}$  release as control (Fig. 6D and E). As a final approach, we measured  $G_q$ PCR-

mediated  $Ca^{2+}$  release from control (PS1<sup>+/+</sup>) and PS1 knockout (PS1<sup>-/-</sup>) mouse embryonic fibroblasts and determined that overnight U18 incubation increased  $G_q$ PCR  $Ca^{2+}$  release in PS1<sup>+/+</sup> cells (Fig. 6F and H) but had no effect on PS1<sup>-/-</sup> cells relative to vehicle

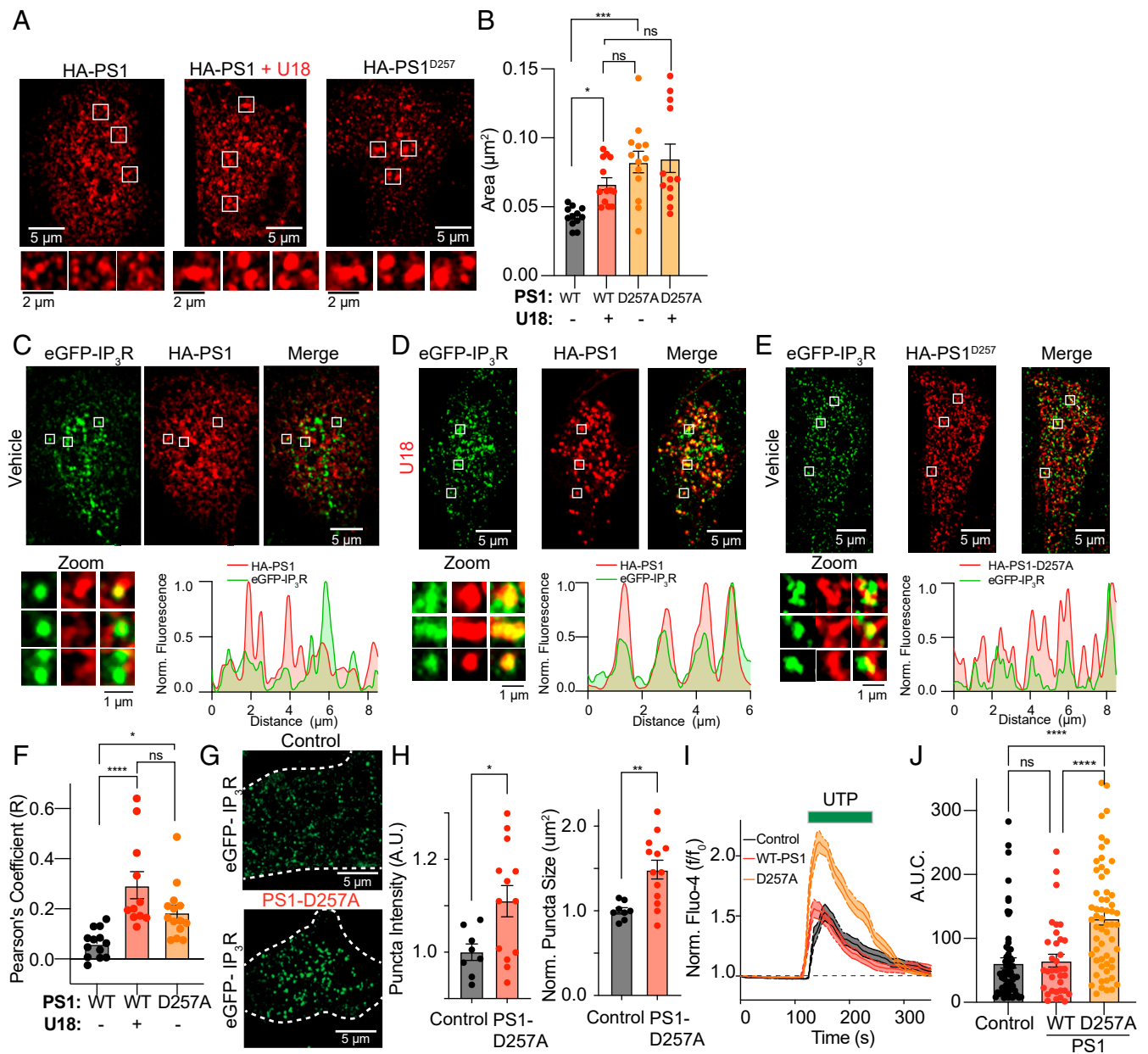


**Fig. 5.** Inhibition of NPC1 increases PS1 clusters and colocalization with IP<sub>3</sub>R1. (A) Representative TIRF images of HeLa cells expressing HA-PS1, HA-PS1 + treated with U18, or HA-PS1<sup>D257A</sup>. (B) Quantification of PS1 area normalized to footprint. (C, Top) TIRF images of eGFP-IP<sub>3</sub>R HeLa cells transfected with HA-PS1-WT. (Bottom) Zoomed regions from solid white squares (Left) and line scan showing distribution of signals (Right). (D) Same as C, only treated with U18. (E) Same as C, only transfected with HA-PS1<sup>D257A</sup>. (F) Quantitative analysis showing average Pearson's correlation coefficients from C–E. (G) Representative TIRF images from Control (Top) and HA-PS1<sup>D257A</sup>-expressing eGFP-IP<sub>3</sub>R HeLa cells. (H) Quantification of IP<sub>3</sub>R1 puncta intensity and size in control and HA-PS1<sup>D257A</sup>-expressing cells. (I) Average time series of Fluo-4 loaded control (black), HA-PS1-expressing (red), and HA-PS1<sup>D257A</sup>-expressing (orange) tsA201 cells treated with UTP (100 μM). (J) Quantitative analysis of the UTP-evoked Ca<sup>2+</sup> area under the curve. All the data are expressed as mean ± SEM from individual cells. Statistical analyses were unpaired t tests except (B) and (F) which were two-way and one-way ANOVAs, respectively. ns: not significant; \*P < 0.05; \*\*P < 0.01; \*\*\*P < 0.001; \*\*\*\*P < 0.0001.

controls (Fig. 6 G and H). Transfecting PS1<sup>-/-</sup> cells with PS1-WT reestablished U-18-mediated increases in G<sub>q</sub>PCR Ca<sup>2+</sup> release (SI Appendix, Fig. S7 A and B). Collectively, these data support the hypothesis that PS1-dependent increases in IP<sub>3</sub>R1 cluster size drive puff activity and G<sub>q</sub>PCR-mediated Ca<sup>2+</sup> release in NPC1 disease.

Previously, we have reported that PS1 levels play a crucial role in decreasing ER Ca<sup>2+</sup> (Ca<sup>2+</sup><sub>ER</sub>) to drive synaptic remodeling of Purkinje neurons in the cerebellum (20). Given the published role that PS1 plays in enhancing the biophysical release properties of IP<sub>3</sub>R1 (32, 31, 34) and the increases in spontaneous Ca<sup>2+</sup><sub>IP<sub>3</sub>R1</sub>

puffs following loss of NPC1 function reported herein, we asked whether IP<sub>3</sub>R1 is downstream of PS1 and involved in decreasing Ca<sup>2+</sup><sub>ER</sub> in NPC1 disease. To begin, we expressed a genetically encoded Ca<sup>2+</sup> indicator targeted to the cytoplasmic leaflet of the ER membrane (Fig. 6I; ER-GCaMP3) in patient fibroblasts, U18-treated tsA cells, or PS1<sup>D257A</sup>-expressing tsA cells to ask whether we could measure steady-state Ca<sup>2+</sup><sub>ER</sub> leak. Aligned with published data (20), both NPC1<sup>I1061T</sup> patient cells (Fig. 6J) and U18-treated tsA201 cells (Fig. 6K) exhibited significantly higher resting ER-GCaMP3 intensity values, consistent with increased Ca<sup>2+</sup><sub>ER</sub>

leak following loss of NPC1 function. To probe a role for PS1–IP<sub>3</sub>R1 interactions facilitating enhanced Ca<sup>2+</sup><sub>ER</sub> leak in NPC1 disease, we performed similar experiments in PS1<sup>-/-</sup> and IP<sub>3</sub>R1<sup>-/-</sup> cell lines and discovered that ER-GCaMP3 intensity values were refractory to U18 treatment under both conditions. These data suggest that PS1 and IP<sub>3</sub>R1 are both key players in increasing Ca<sup>2+</sup><sub>ER</sub> leak in NPC1 disease.

The consequence of increased Ca<sup>2+</sup><sub>ER</sub> leak is a decrease in free Ca<sup>2+</sup><sub>ER</sub> concentrations in NPC1 loss-of-function cells (20); thus, we tested the effect of knocking out IP<sub>3</sub>R1 (Fig. 6O). We loaded NPC1<sup>-/-</sup> cells and IP<sub>3</sub>R1<sup>-/-</sup> cells with the cytosolic Ca<sup>2+</sup> dye, Fluo-4, and applied the SERCA inhibitor thapsigargin in a 0-mM, Ca<sup>2+</sup>-containing extracellular solution. Treatment with thapsigargin gave the expected increase in cytoplasmic fluo-4 intensity from control cells, with NPC1<sup>-/-</sup> cells having a smaller increase in intensity (20) (Fig. 6P and Q). Conducting similar experiments in IP<sub>3</sub>R1<sup>-/-</sup> cells treated with vehicle control or U18 did not result in any significant differences in fluo-4 intensity following Thapsigargin treatment and provide evidence that increased PS1–IP<sub>3</sub>R1 interactions drives decreased Ca<sup>2+</sup><sub>ER</sub> in NPC1 disease (Fig. 6R and S).

**Inhibition of SREBP Prevents Increases in IP<sub>3</sub>R1 Cluster Size and G<sub>q</sub>PCR Ca<sup>2+</sup> Following Loss of NPC1 Function.** Loss of NPC1 function decreases lysosomal to ER cholesterol transport, resulting in depletion of ER membrane cholesterol and subsequent activation of the sterol regulatory element binding protein (SREBP) pathway, leading to increased gene expression of SREBP-dependent targets (35). We have previously reported that increased SREBP activity in NPC1 loss-of-function cells up-regulates expression of several Ca<sup>2+</sup>-handling proteins, including PS1, with inhibition of the SREBP pathway reversing differential protein expression along with aberrant ER Ca<sup>2+</sup> and SOCE phenotypes (20). Thus, we wanted to determine whether the SREBP pathway is involved in the remodeling of IP<sub>3</sub>Rs and potentiated G<sub>q</sub>PCR-mediated Ca<sup>2+</sup> release. To begin, we conducted qPCR experiments on NPC1<sup>11061T</sup> cells to determine whether mRNA levels of each IP<sub>3</sub>R isoform are altered. Consistent with Western blot data, mRNA levels for IP<sub>3</sub>R1, but not IP<sub>3</sub>R2 or IP<sub>3</sub>R3, were increased in NPC1<sup>11061T</sup> cells (Fig. 7A). Treating cells overnight with the SREBP inhibitor, PF-429242 (500 nM), abolished increases in IP<sub>3</sub>R1 levels from NPC1<sup>11061T</sup> cells without affecting steady-state mRNA levels of IP<sub>3</sub>R2 or IP<sub>3</sub>R3. Furnished with the information that PF-429242 can decrease IP<sub>3</sub>R1 mRNA levels, we next asked whether PF-429242 treatment rescues IP<sub>3</sub>R1 cluster size in NPC1 loss-of-function cells. To answer this question, we treated eGFP-IP<sub>3</sub>R1 cells with U18, or U18 and PF-429242, before quantifying IP<sub>3</sub>R1 clusters using TIRF microscopy (Fig. 7B). Similar to the observed decreases in mRNA levels, treatment with PF-429242 decreased IP<sub>3</sub>R1 cluster size back to control levels (Fig. 7C). Next, we measured G<sub>q</sub>PCR-mediated Ca<sup>2+</sup> release to test whether PF-429242-mediated decreases in IP<sub>3</sub>R1 mRNA and cluster size would also decrease Ca<sup>2+</sup> release. Analysis of intracellular Fluo-4 intensity following application of histamine determined that PF-429242 reduces the G<sub>q</sub>PCR evoked Ca<sup>2+</sup> signal in NPC1 fibroblasts back to healthy fibroblast control levels. Finally, we conducted G<sub>q</sub>PCR experiments in SCAP<sup>-/-</sup> cells that lack a functional SREBP pathway (36) and found that U18 treatment resulted in a slight decrease in Ca<sup>2+</sup> release following receptor activation (Fig. 7F and G). Therefore, like other Ca<sup>2+</sup>-handling proteins that are increased in NPC1 disease, IP<sub>3</sub>R1 can be normalized back to control levels following inhibition of SREBP.

**IP<sub>3</sub>R1 Drives Ca<sup>2+</sup>-Dependent NFAT Translocation and Cytotoxic Elevations in Mitochondrial Ca<sup>2+</sup> Following Loss of NPC1 Function.** Finally, we wanted to begin elucidating the cellular consequences of aberrant nanoscale distribution and activity of the IP<sub>3</sub>R in NPC1 disease. Because alterations in cytoplasmic Ca<sup>2+</sup> and IP<sub>3</sub>R-mediated

Ca<sup>2+</sup> release are fundamentally required for many cellular processes, we focused on two of these pathways: NFAT signaling (37) and mitochondrial Ca<sup>2+</sup> (13) (Ca<sup>2+</sup><sub>Mito</sub>) to ask whether they are altered in NPC1 disease.

NFAT proteins are a family of transcription factors who are phosphorylated and reside in the cytoplasm. Upon IP<sub>3</sub>R stimulation to simultaneously elevate intracellular Ca<sup>2+</sup> concentrations and deplete Ca<sup>2+</sup><sub>ER</sub>, thereby activating store-operated Ca<sup>2+</sup> entry, NFATs are dephosphorylated by the Ca<sup>2+</sup>/calmodulin-dependent serine phosphatase, calcineurin, and translocate to the nucleus to become active (Fig. 8A). First, we tested whether steady-state NFAT distribution is different between control and NPC1<sup>11061T</sup> cells; analysis of fluorescence intensity ratios between the cytoplasm and nucleus revealed that NPC1<sup>11061T</sup> cells had a small but significant increase in the proportion of NFAT in the nucleus (Fig. 8B and C). A similar distribution was observed in U18-treated cells (Fig. 8D). To test whether IP<sub>3</sub>R1 is involved in mediating steady-state increases in nuclear NFAT in NPC1 loss-of-function cells, we performed similar experiments in IP<sub>3</sub>R1<sup>-/-</sup> cells. Quantification of NFAT cytoplasmic/nuclear intensities from U18-treated IP<sub>3</sub>R1<sup>-/-</sup> disclosed that NFAT no longer preferentially accumulated in the nucleus at steady-state (Fig. 8D). Next, we tested whether G<sub>q</sub>PCR-stimulated NFAT translocation was also different between control and NPC1<sup>11061T</sup> patient cells. Time series analysis revealed that 100-s histamine application, a stimulus that increases cytoplasmic Ca<sup>2+</sup> (Fig. 1F), increased NFAT more quickly in the nucleus of NPC1<sup>11061T</sup> cells relative to control (Fig. 8E). Thus, there is a correlation between the amount of G<sub>q</sub>PCR-Ca<sup>2+</sup> release and NFAT translocation. To probe the involvement of IP<sub>3</sub>R1, we repeated experiments in tsA201 cells and IP<sub>3</sub>R1<sup>-/-</sup> cells treated with U18. Similar to NPC1<sup>11061T</sup> patient cells, treatment of tsA201 cells with U18 significantly increased NFAT translocation to the nucleus (Fig. 8F), an increase that was completely absent in IP<sub>3</sub>R1<sup>-/-</sup> cells (Fig. 8G). These experiments provide evidence that NPC1-dependent increases in IP<sub>3</sub>R1 increase NFAT signaling in NPC1 disease.

As a final test to determine the cellular consequences of altered IP<sub>3</sub>R1 signaling in NPC1 disease, we investigated Ca<sup>2+</sup><sub>Mito</sub> and cell viability. Ca<sup>2+</sup> represents a key rheostat that couples mitochondria biogenetics to cellular demand and is frequently altered in pathophysiological conditions, including neurodegeneration. Intimate interactions between VDAC1 on mitochondria membranes and IP<sub>3</sub>R1 on ER membranes provide the platform for constitutive IP<sub>3</sub>R-mediated Ca<sup>2+</sup> release to maintain cellular bioenergetics to meet cellular demands (38) (Fig. 8H). Given the importance of IP<sub>3</sub>R1 in regulating Ca<sup>2+</sup><sub>Mito</sub>, we expressed a genetically encoded Ca<sup>2+</sup> indicator targeted to mitochondria (Mito-RCaMP1) to ask whether Ca<sup>2+</sup><sub>Mito</sub> is altered following loss of NPC1 function. Quantification of Mito-RCaMP1 intensities between cells treated with a vehicle or U18 revealed that loss of NPC1 function significantly increased Ca<sup>2+</sup><sub>Mito</sub> (Fig. 8I and J). Identical experiments conducted on IP<sub>3</sub>R1<sup>-/-</sup> cells revealed reduced Ca<sup>2+</sup><sub>Mito</sub> levels compared to control with IP<sub>3</sub>R1<sup>-/-</sup> cells now being refractory to U18 treatment (Fig. 8J). In parallel, we asked whether increases in Ca<sup>2+</sup><sub>Mito</sub>, which can be cytotoxic in neurodegenerative conditions, are accompanied by changes in cell health. Consistent with this hypothesis, cell viability assays determined U18-dependent increases in Ca<sup>2+</sup><sub>Mito</sub> correlated with increased cell death (Fig. 8K), an observation that was completely absent in IP<sub>3</sub>R1<sup>-/-</sup> cells. Collectively, these data suggest that NPC1-dependent increases in IP<sub>3</sub>R1 distribution/activity increase Ca<sup>2+</sup><sub>Mito</sub> cytotoxicity in NPC1 disease and presents the IP<sub>3</sub>R as a potential target to slow neurodegeneration.

## Discussion

Dysfunction of IP<sub>3</sub>Rs is a common feature across many neurodegenerative diseases (39–41); thus, determining molecular details regarding their regulation and control is imperative for



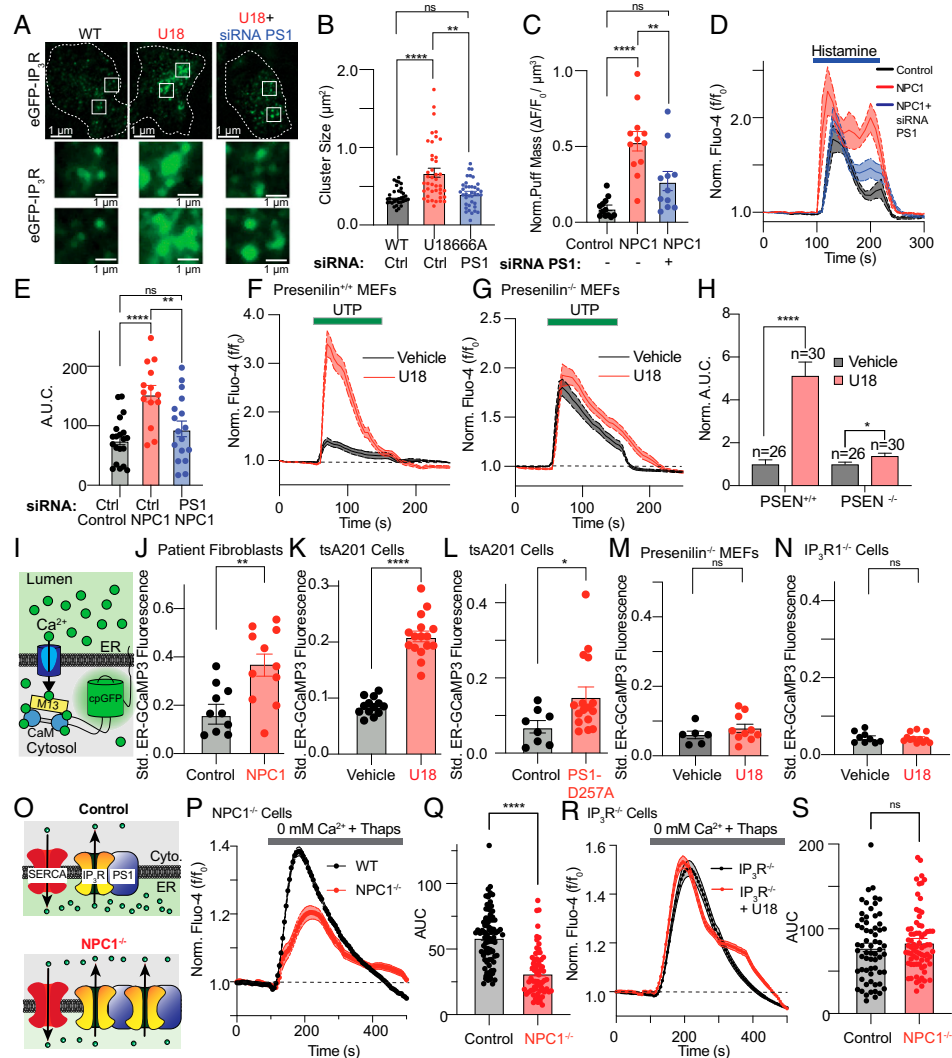


**Fig. 6.** Knocking out PS1 or IP<sub>3</sub>R1 rescues Ca<sup>2+</sup> defects in NPC1 disease cells. (A) Representative TIRF images from control, U18-treated, and U18-treated + siRNA PS1 eGFP-IP<sub>3</sub>R1 cells. Zoomed areas are taken from the solid white squares. (B) Quantification of eGFP-IP<sub>3</sub>R1 cluster size. (C) Quantification of spontaneous Ca<sup>2+</sup> activity. (D) Average time series of histamine responses from Fluo-4 loaded control (black), NPC1<sup>11061T</sup> (red), and NPC1<sup>11061T</sup> + siRNA PS1 (blue) fibroblasts. (E) Quantitative analysis of the histamine-evoked Ca<sup>2+</sup> area under the curve (A.U.C.). (F) Average time series of UTP responses from Fluo-4 loaded PSEN<sup>+/+</sup> MEF cells treated with vehicle control (black) or U18 (red). (G) Same as F, only PS1<sup>-/-</sup> cells. (H) Quantification of UTP-evoked Fluo-4 signals. (I) Schematic of genetically encoded ER-GCaMP3 Ca<sup>2+</sup> indicator. (J) Quantification of normalized ER-GCaMP3 intensity in patient fibroblasts. (K) Same as J, only tsA201 cells treated with U18. (L) Same as K, only tsA201 cells expressing PS1<sup>D257A</sup>. (M) Same as K, only PS1<sup>-/-</sup> cells. (N) Same as K, only IP<sub>3</sub>R1<sup>-/-</sup> cells. (O) Schematic of IP<sub>3</sub>R1-PS1 hypothesis in NPC1 disease. (P) Average time series of thapsigargin responses from Fluo-4 loaded control (black line) and NPC1<sup>-/-</sup> (red line) cells. (Q) Quantification of area under thapsigargin responses. (R) Same as P, except IP<sub>3</sub>R1<sup>-/-</sup> cells. (S) Same as Q. All the data are expressed as mean ± SEM from individual cells. B, C, and E were one-way ANOVAs; H was a two-way ANOVA; and J–N, Q, and S were unpaired t tests. ns: not significant; \*P < 0.05; \*\*P < 0.01; \*\*\*\*P < 0.0001.

human health. Here, we discover a signaling axis that links the NPC1 lysosomal cholesterol transporter to the nanoscale distribution and activity of IP<sub>3</sub>R1 (SI Appendix, Fig. S8). We show that loss of NPC1 function results in augmented clustering of IP<sub>3</sub>R1 near the PM, increased frequency and size of spontaneous Ca<sup>2+</sup> puffs from IP<sub>3</sub>R1s, and enhanced G<sub>q</sub>PCR-mediated intracellular Ca<sup>2+</sup> signaling. Upstream of changes in IP<sub>3</sub>R1 appears to be PS1, with overexpression of PS1<sup>D257A</sup> phenocopying the observed changes in NPC1 disease cells. Mechanistically linking cholesterol egress from the lysosome to IP<sub>3</sub>R1-dependent alterations in Ca<sup>2+</sup> is the SREBP pathway, with inhibition of this transcription pathway restoring mRNA levels, IP<sub>3</sub>R1 cluster size, and G<sub>q</sub>PCR signaling, respectively. Functionally, altered IP<sub>3</sub>R1 distribution/activity leads to increased steady-state and stimulated Ca<sup>2+</sup>-dependent NFAT signaling and Ca<sup>2+</sup><sub>mito</sub> toxicity.

G<sub>q</sub>PCRs are pivotal purveyors of physiological information, transducing fluctuations in hormones, growth factors, and neurotransmitters across the PM to stimulate intracellular second messengers that initiate downstream signaling cascades. In this study, we determine that the PM-localized elements of G<sub>q</sub>PCR signaling cascades, namely receptor, G<sub>q</sub>, and PLC, are unaltered or, in the case of PI(4,5)P<sub>2</sub>, decreased (19) following loss of NPC1 function. These observations, coupled with decreased Ca<sup>2+</sup><sub>ER</sub> levels (20), made it surprising to find that both receptor-activated and spontaneous IP<sub>3</sub>R1-mediated Ca<sup>2+</sup> responses are amplified in NPC1 disease cells. This counterintuitive discovery can be reconciled with information that IP<sub>3</sub>R1 protein abundance, nanoscale distribution, mobility near the PM, and activity are all enhanced in NPC1 disease. The degree of spatial, temporal, and allosteric plasticity exhibited by IP<sub>3</sub>R1 has been previously reported

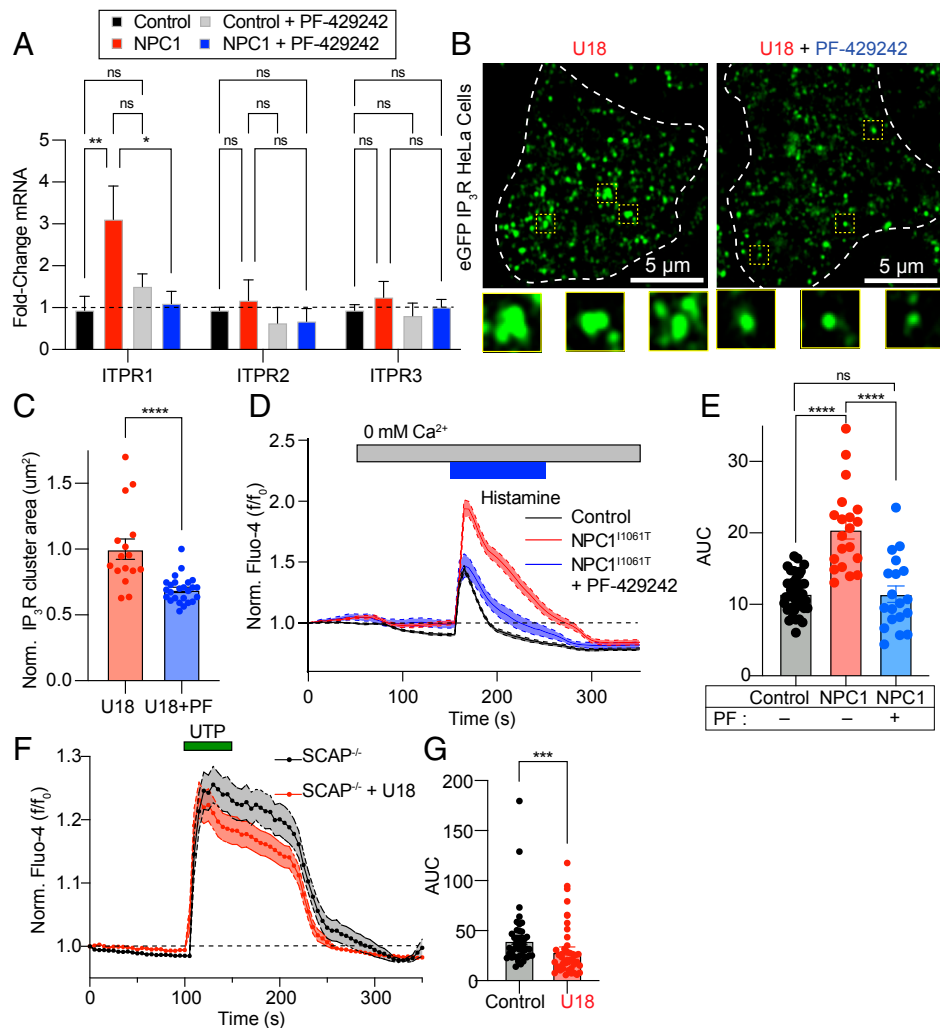


**Fig. 7.** Inhibition or loss of SREBP pathway activity rescues expression and distribution of IP<sub>3</sub>R1 and Ca<sup>2+</sup> phenotypes in NPC1 disease. (A) Quantification of ITPR1, ITPR2, and ITPR3 mRNA levels in control (black), control + PF-429242 (gray), NPC1<sup>11061T</sup> (red), and NPC1<sup>11061T</sup> + PF-429242 (blue) patient fibroblasts. (B) Representative TIRF images from eGFP-IP<sub>3</sub>R1 HeLa cells treated with U18 (Left) or U18 and PF-429242. (C) Quantification of IP<sub>3</sub>R1 cluster size. (D) Average time series of histamine responses from Fluo-4 loaded control (black line), NPC1<sup>11061T</sup> (red line) cells, and NPC1<sup>11061T</sup> + PF429242 fibroblasts. (E) Quantification of area under the histamine responses. (F) Average time series of UTP responses from Fluo-4 loaded control (black line) or U18-treated (red line) SCAP<sup>-/-</sup> cells. (G) Quantification of area under the UTP responses. All the data are expressed as mean ± SEM from individual cells. Statistical significance was calculated using the following test: A, two-way ANOVA; C and G, unpaired *t* tests; and E, one-way ANOVA. ns: not significant; \**P* < 0.05; \*\**P* < 0.01; \*\*\**P* < 0.001; \*\*\*\**P* < 0.0001.

(25, 31, 42); we add another modulatory mechanism for IP<sub>3</sub>R1 and G<sub>q</sub>PCR-mediated Ca<sup>2+</sup> release through NPC1 abundance and/or cholesterol egress across lysosomal-ER MCS. This positions NPC1 and lysosomal-ER MCS as potential targets to tune G<sub>q</sub>PCR signaling with the goal of altering global or local Ca<sup>2+</sup> release to modify neuronal bioenergetics, Ca<sup>2+</sup>-dependent transcription, or synaptic plasticity in health or disease.

We detail an important role for PS1 in regulating IP<sub>3</sub>R1 distribution and activity following loss of NPC1 function. Under normal physiological conditions, PS1 undergoes autoproteolytic cleavage, resulting in two fragments (N and C terminals) that associate with other proteins to create the γ-secretase complex. Several mutations in the gene encoding PS1 can abolish this autoproteolytic activity, keeping PS1 in an uncleaved and full-length state, which is purported to form Ca<sup>2+</sup> leak channels at the ER membrane (33). Contrasting the hypothesis that PS1 is a Ca<sup>2+</sup> leak channel, Cheung et al. have reported that both Familial Alzheimer's Disease-linked PS1 mutations, which lack the ER Ca<sup>2+</sup> leak activity, as well as the catalytically dead PS1 mutants that maintain their full uncleaved length bind and enhance the gating properties of IP<sub>3</sub>Rs (31),

suggesting the mechanism of Ca<sup>2+</sup><sub>ER</sub> leak involves physical interactions between PS1 and IP<sub>3</sub>R1. We find that PS1 and IP<sub>3</sub>Rs have little colocalization after overexpression of wild-type PS1; however, inhibition of NPC1 significantly increased their localization with one another. Additionally, overexpression of the catalytically dead PS1<sup>D257A</sup> mutation that results in increased full-length protein form reorganizes IP<sub>3</sub>R1 nanoscale distribution, spontaneous puff activity, and G<sub>q</sub>PCR-mediated Ca<sup>2+</sup> release, independent of NPC1 inhibition. Finally, IP<sub>3</sub>R1<sup>-/-</sup> cells are refractory to U18 with no NPC1-dependent Ca<sup>2+</sup> phenotypes. This leads us to suggest that it is the physical interactions between PS1 and IP<sub>3</sub>R1, coupled with elevations in cytoplasmic Ca<sup>2+</sup> (20), that modify the clustering properties of IP<sub>3</sub>R1 to enhance their cooperative gating and thereby their release probability in NPC disease. If this model is correct, it would position IP<sub>3</sub>R1-mediated Ca<sup>2+</sup> release as the distal element underlying enhanced Ca<sup>2+</sup><sub>ER</sub> leak in NPC1 disease. Questions remain to fully determine the molecular choreography of PS1-IP<sub>3</sub>R1 complex, including the following: 1) What is the optimal stoichiometry of PS1-IP<sub>3</sub>R1 interactions? 2) Do decreases in IP<sub>3</sub>R1 mobility act as a diffusion trap for PS1 to bind,

aggregate, and influence IP<sub>3</sub>R? 3) Does decreased ER cholesterol in NPC1 cells, as evidenced by enhanced SREBP processing (20), reduce cholesterol-dependent partitioning of PS1 and IP<sub>3</sub>R to allow their increased clustering/interaction? and 4) Are there other accessory proteins that exert regulatory influence over this signaling complex?

The SREBP transcription factor appears to link changes in NPC1 function to alterations in IP<sub>3</sub>R1 and G<sub>q</sub>PCR signaling. Previously, we have reported that the SREBP pathway is involved in mediating expressional changes in the Ca<sup>2+</sup>-handling proteins SERCA, STIM1, ORAI1, and PS1 in NPC1<sup>I1061T</sup> cells; therefore, it is perhaps not surprising that the IP<sub>3</sub>R1 is also influenced by SREBP. That being said, it is still unknown whether regulation of IP<sub>3</sub>R1 by SREBP is through direct or indirect transcriptional regulation. Further, a key question that remains unanswered is whether alterations in intracellular Ca<sup>2+</sup> signaling are purely deleterious sequences (see paragraph below) or are part of a molecular mechanism(s) attempting to correct the cellular phenotypes of NPC1 disease. There are clear links between elevations in intracellular Ca<sup>2+</sup> levels and endocytic fusion and transport events; further, decreasing Ca<sup>2+</sup><sub>ER</sub> has been reported to redistribute the intracellular pool of unesterified cholesterol (43) and rescue key cellular phenotypes of NPC1 disease (6), while knocking out INPP5A (44) (IP<sub>3</sub> 5-phosphatase) triggers depletion of cellular cholesterol. Thus, changes in Ca<sup>2+</sup><sub>ER</sub> signaling may be a key rheostat for maintenance and control of cellular cholesterol homeostasis.

Ca<sup>2+</sup>-handling proteins have been linked to a host of pathologies, including several neurodegenerative disorders (33, 34). MCS between the ER and mitochondrial are regions of intimate membrane apposition that facilitate transport of Ca<sup>2+</sup> from the ER to the mitochondria. Following G<sub>q</sub>PCR activation or spontaneous IP<sub>3</sub>R opening, Ca<sup>2+</sup> is taken up into mitochondria to participate in the control of bioenergetics by activating oxidative metabolism, mitochondrial respiration, and ATP synthesis. Notably, dysregulation of Ca<sup>2+</sup><sub>Mito</sub> are potent triggers of necrosis, apoptosis, and autophagy (for review, refer to ref. 45). Here, we present evidence that NPC1-dependent increases in IP<sub>3</sub>R1 distribution and activity increase Ca<sup>2+</sup><sub>Mito</sub> to enhance cell death in NPC1 disease models. Thus, although increased Ca<sup>2+</sup> release from the ER may be initiated as a mechanism to alter cholesterol homeostasis or redistribute toxic metabolites associated with NPC1 disease mutations, the prolonged elevations in cytoplasmic and Ca<sup>2+</sup><sub>Mito</sub> could ultimately be a central driver of neuronal cell death in NPC disease. This presents IP<sub>3</sub>R1 and MAMs as potential therapeutic targets to correct Ca<sup>2+</sup> phenotypes in order to slow Purkinje neuron neurodegeneration and NPC disease progression.

In conclusion, we characterize a link between the lysosomal NPC1 cholesterol transporter and changes in IP<sub>3</sub>R-dependent Ca<sup>2+</sup> signaling. We find that differential expressional and localization of IP<sub>3</sub>R1 enhances both spontaneous and G<sub>q</sub>PCR-mediated Ca<sup>2+</sup> release to promote mitochondrial cytotoxicity. This work furthers our understanding of the regulatory factors that tune IP<sub>3</sub>R

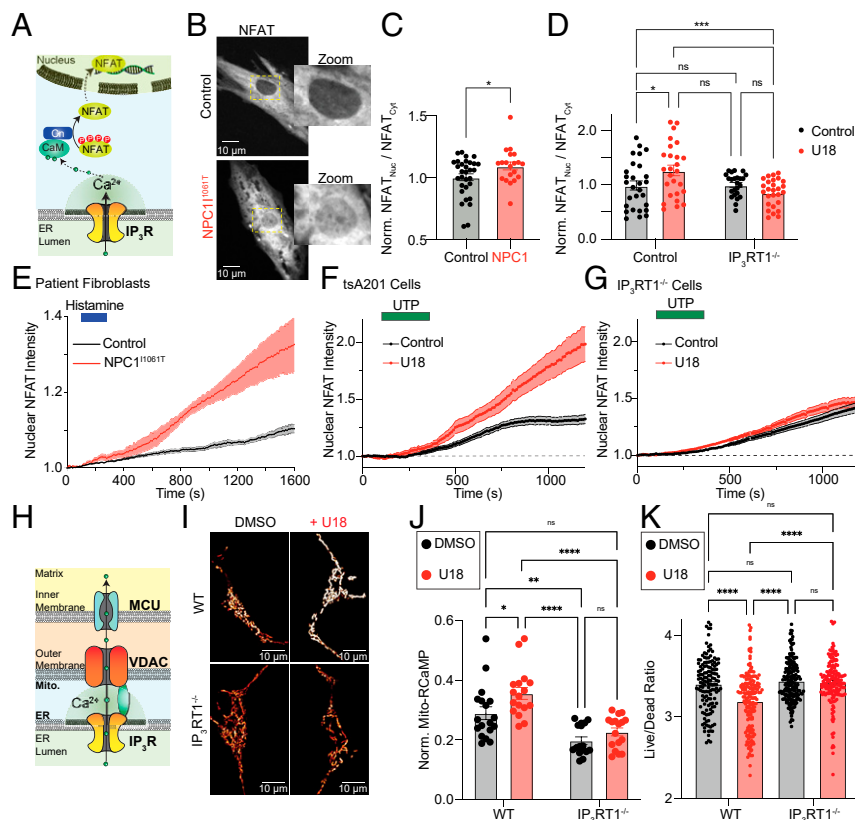


**Fig. 8.** Knockout of IP<sub>3</sub>R1 rescues Ca<sup>2+</sup>-dependent gene transcription and Ca<sup>2+</sup><sub>Mito</sub> cytotoxicity in NPC1 loss-of-function cells. (A) Schematic of NFAT translocation to the nucleus. (B) Representative images from control (Top) and NPC1<sup>I1061T</sup> (Bottom) fibroblasts expressing NFAT. (C) Quantification of NFAT intensity in the nucleus relative to the cytoplasm in control and NPC1<sup>I1061T</sup> fibroblasts. (D) Same analysis as C, only using control and IP<sub>3</sub>R1<sup>-/-</sup> cells. (E) Averaged time series of nuclear NFAT intensity following the addition of Histamine in control (black line) and NPC1<sup>I1061T</sup> (red line) fibroblasts. (F) Same as E, only UTP application in control and U18-treated tsA201 cells. (G) Same as F, only using IP<sub>3</sub>R1<sup>-/-</sup> cells. (H) Schematic of Ca<sup>2+</sup> transfer at ER-mitochondria MCS. (I) Representative images of Mito-RCaMP in control (Top) and IP<sub>3</sub>R1<sup>-/-</sup> cells (Bottom) treated with vehicle control (Left) or U18 (Right). (J) Quantification of normalized Mito-RCaMP intensity in control and IP<sub>3</sub>R1<sup>-/-</sup> cells. (K) Quantification of live cell/dead cell ratio in control and IP<sub>3</sub>R1<sup>-/-</sup> cells treated with vehicle control or U18. All the data are expressed as mean ± SEM from individual cells. Statistical significance was calculated using the following tests: C, unpaired t test and D, J, and K, two-way ANOVA. ns: not significant; \*P < 0.05; \*\*P < 0.01; \*\*\*\*P < 0.0001.

signaling, most importantly PS1, whose form and expression are altered in NPC1 disease. By elucidating these regulatory pathways, we have provided potential therapeutic targets to address IP<sub>3</sub>R dysfunction, a feature of NPC1 disease and other neurodegenerative disorders.

## Materials and Methods

Detailed methods can be found in *SI Appendix*. Briefly, NPC1<sup>I1061T</sup> patient cells, NPC1<sup>-/-</sup> cells, and tsA201 cells treated overnight with U18666A and male and female NPC1<sup>I1061T</sup> mice served as models of NPC disease and were compartmented to control cells in this study. Protein levels were determined using immunoblot approaches. Ca<sup>2+</sup> imaging was performed using an Andor W1 spinning disk system. Immunofluorescence TIRF, superresolution, and

confocal images were acquired using a Leica single-molecule localization system or a Zeiss AiryScan confocal microscope.

**Data Availability.** All study data are included in the article and/or *SI Appendix*.

**ACKNOWLEDGMENTS.** We are extremely grateful to those laboratories that shared reagents, plasmids, and cells lines used in this study. We thank Dr. Oscar Vivas for technical assistance. This work was supported by an Ara Parseghian Medical Research Foundation award (E.J.D.); University of California funds (E.J.D.); NIH grant R01 GM127513 (E.J.D.); NIH T32 training award T32GM099608 (S.A.T.); and NIH grants R01 NS114210 and HL144071 (L.F.S.), R01 NS109176 (S.S.), R01 HL06773 (D.S.O.), and R01 AG063796 (R.E.D.).

1. A. Ghosh, M. E. Greenberg, Calcium signaling in neurons: Molecular mechanisms and cellular consequences. *Science* **268**, 239–247 (1995).
2. I. Bezprozvanny, Calcium signaling and neurodegenerative diseases. *Trends Mol. Med.* **15**, 89–100 (2009).
3. J. K. Foskett, C. White, K.-H. Cheung, D.-O. D. Mak, Inositol trisphosphate receptor Ca<sup>2+</sup> release channels. *Physiol. Rev.* **87**, 593–658 (2007).
4. D. L. Prole, C. W. Taylor, Structure and function of IP<sub>3</sub> receptors. *Cold Spring Harb. Perspect. Biol.* **11**, 11–17 (2019).
5. S. A. Tiscione *et al.*, Disease-associated mutations in Niemann-Pick type C1 alter ER calcium signaling and neuronal plasticity. *J. Cell Biol.* **218**, 4141–4156 (2019).
6. E. Lloyd-Evans *et al.*, Niemann-Pick disease type C1 is a sphingosine storage disease that causes deregulation of lysosomal calcium. *Nat. Med.* **14**, 1247–1255 (2008).
7. D. Shen *et al.*, Lipid storage disorders block lysosomal trafficking by inhibiting a TRP channel and lysosomal calcium release. *Nat. Commun.* **3**, 731 (2012).
8. M. J. Berridge, Calcium hypothesis of Alzheimer's disease. *Pflügers Arch.* **459**, 441–449 (2010).
9. T. Furuichi *et al.*, Widespread expression of inositol 1,4,5-trisphosphate receptor type 1 gene (*Insp3r1*) in the mouse central nervous system. *Receptors Channels* **1**, 11–24 (1993).
10. J. R. Sarna *et al.*, Patterned Purkinje cell degeneration in mouse models of Niemann-Pick type C disease. *J. Comp. Neurol.* **456**, 279–291 (2003).
11. M. J. Berridge, The inositol trisphosphate/calcium signaling pathway in health and disease. *Physiol. Rev.* **96**, 1261–1296 (2016).
12. T. Inoue, K. Kato, K. Kohda, K. Mikoshiba, Type 1 inositol 1,4,5-trisphosphate receptor is required for induction of long-term depression in cerebellar Purkinje neurons. *J. Neurosci.* **18**, 5366–5373 (1998).
13. R. Rizzuto *et al.*, Close contacts with the endoplasmic reticulum as determinants of mitochondrial Ca<sup>2+</sup> responses. *Science* **280**, 1763–1766 (1998).
14. M. Matsumoto *et al.*, Ataxia and epileptic seizures in mice lacking type 1 inositol 1,4,5-trisphosphate receptor. *Nature* **379**, 168–171 (1996).
15. C. Hisatsune *et al.*, IP<sub>3</sub>R1 deficiency in the cerebellum/brainstem causes basal ganglia-independent dystonia by triggering tonic Purkinje cell firings in mice. *Front. Neural Circuits* **7**, 156 (2013).
16. J. van de Leemput *et al.*, Sequencing analysis of the ITPR1 gene in a pure autosomal dominant spinocerebellar ataxia series. *Mov. Disord.* **25**, 771–773 (2010).
17. S. Barresi *et al.*, Mutations in the IRBIT domain of ITPR1 are a frequent cause of autosomal dominant nonprogressive congenital ataxia. *Clin. Genet.* **91**, 86–91 (2017).
18. S. Gerber *et al.*, Recessive and dominant de novo ITPR1 mutations cause Gillespie syndrome. *Am. J. Hum. Genet.* **98**, 971–980 (2016).
19. O. Vivas, S. A. Tiscione, R. E. Dixon, D. S. Ory, E. J. Dickson, Niemann-Pick type C disease reveals a link between lysosomal cholesterol and PtdIns(4,5)P<sub>2</sub> that regulates neuronal excitability. *Cell Rep.* **27**, 2636–2648.e4 (2019).
20. S. A. Tiscione *et al.*, Disease-associated mutations in Niemann-Pick type C1 alter ER calcium signaling and neuronal plasticity. *J. Cell Biol.* **218**, 4141–4156 (2019).
21. F. Lu *et al.*, Identification of NPC1 as the target of U18666A, an inhibitor of lysosomal cholesterol export and Ebola infection. *eLife* **4**, e12177 (2015).
22. M. Praggastis *et al.*, A murine Niemann-Pick C1 I1061T knock-in model recapitulates the pathological features of the most prevalent human disease allele. *J. Neurosci.* **35**, 8091–8106 (2015).
23. Y. Higashi, S. Murayama, P. G. Pentchev, K. Suzuki, Cerebellar degeneration in the Niemann-Pick type C mouse. *Acta Neuropathol.* **85**, 175–184 (1993).
24. E. J. Dickson, B. H. Falkenburger, B. Hille, Quantitative properties and receptor reserve of the IP<sub>3</sub> and calcium branch of G<sub>q</sub>-coupled receptor signaling. *J. Gen. Physiol.* **141**, 521–535 (2013).
25. Taufiq-Ur-Rahman, A. Skupin, M. Falcke, C. W. Taylor, Clustering of InsP<sub>3</sub> receptors by InsP<sub>3</sub> retunes their regulation by InsP<sub>3</sub> and Ca<sup>2+</sup>. *Nature* **458**, 655–659 (2009).
26. C. W. Taylor, S. C. Tovey, IP(3) receptors: toward understanding their activation. *Cold Spring Harb. Perspect. Biol.* **2**, a004010 (2010).
27. T. Rahman, C. W. Taylor, Nuclear patch-clamp recording from inositol 1,4,5-trisphosphate receptors. *Methods Cell Biol.* **99**, 199–224 (2010).
28. N. B. Thillaipappan, A. P. Chavda, S. C. Tovey, D. L. Prole, C. W. Taylor, Ca<sup>2+</sup> signals initiate at immobile IP<sub>3</sub> receptors adjacent to ER-plasma membrane junctions. *Nat. Commun.* **8**, 1505 (2017).
29. E. J. Dickson *et al.*, Dynamic formation of ER-PM junctions presents a lipid phosphatase to regulate phosphoinositides. *J. Cell Biol.* **213**, 33–48 (2016).
30. G. D. Dickinson, D. Swaminathan, I. Parker, The probability of triggering calcium puffs is linearly related to the number of inositol trisphosphate receptors in a cluster. *Biophys. J.* **102**, 1826–1836 (2012).
31. K. H. Cheung *et al.*, Mechanism of Ca<sup>2+</sup> disruption in Alzheimer's disease by presenilin regulation of InsP<sub>3</sub> receptor channel gating. *Neuron* **58**, 871–883 (2008).
32. D. Shilling *et al.*, Suppression of InsP<sub>3</sub> receptor-mediated Ca<sup>2+</sup> signaling alleviates mutant presenilin-linked familial Alzheimer's disease pathogenesis. *J. Neurosci.* **34**, 6910–6923 (2014).
33. H. Tu *et al.*, Presenilins form ER Ca<sup>2+</sup> leak channels, a function disrupted by familial Alzheimer's disease-linked mutations. *Cell* **126**, 981–993 (2006).
34. G. E. Stutzmann, A. Caccamo, F. M. LaFerla, I. Parker, Dysregulated IP<sub>3</sub> signaling in cortical neurons of knock-in mice expressing an Alzheimer's-linked mutation in presenilin1 results in exaggerated Ca<sup>2+</sup> signals and altered membrane excitability. *J. Neurosci.* **24**, 508–513 (2004).
35. M. S. Brown, J. L. Goldstein, The SREBP pathway: Regulation of cholesterol metabolism by proteolysis of a membrane-bound transcription factor. *Cell* **89**, 331–340 (1997).
36. R. B. Rawson, R. DeBose-Boyd, J. L. Goldstein, M. S. Brown, Failure to cleave sterol regulatory element-binding proteins (SREBPs) causes cholesterol auxotrophy in Chinese hamster ovary cells with genetic absence of SREBP cleavage-activating protein. *J. Biol. Chem.* **274**, 28549–28556 (1999).
37. M. F. Gomez, A. S. Stevenson, A. D. Bonev, D. C. Hill-Eubanks, M. T. Nelson, Opposing actions of inositol 1,4,5-trisphosphate and ryanodine receptors on nuclear factor of activated T-cells regulation in smooth muscle. *J. Biol. Chem.* **277**, 37756–37764 (2002).
38. C. Cárdenas *et al.*, Essential regulation of cell bioenergetics by constitutive InsP<sub>3</sub> receptor Ca<sup>2+</sup> transfer to mitochondria. *Cell* **142**, 270–283 (2010).
39. C. Hisatsune, K. Mikoshiba, IP<sub>3</sub> receptor mutations and brain diseases in human and rodents. *J. Neurochem.* **141**, 790–807 (2017).
40. P. Egorova, E. Popugaeva, I. Bezprozvanny, Disturbed calcium signaling in spinocerebellar ataxias and Alzheimer's disease. *Semin. Cell Dev. Biol.* **40**, 127–133 (2015).
41. I. Bezprozvanny, Role of inositol 1,4,5-trisphosphate receptors in pathogenesis of Huntington's disease and spinocerebellar ataxias. *Neurochem. Res.* **36**, 1186–1197 (2011).
42. J. Shuai, H. J. Rose, I. Parker, The number and spatial distribution of IP<sub>3</sub> receptors underlying calcium puffs in *Xenopus* oocytes. *Biophys. J.* **91**, 4033–4044 (2006).
43. W. A. Wang *et al.*, Loss of calreticulin uncovers a critical role for calcium in regulating cellular lipid homeostasis. *Sci. Rep.* **7**, 5941 (2017).
44. M. Malek *et al.*, Inositol triphosphate-triggered calcium release blocks lipid exchange at endoplasmic reticulum-Golgi contact sites. *Nat. Commun.* **12**, 2673 (2021).
45. C. Giorgi, S. Marchi, P. Pinton, The machineries, regulation and cellular functions of mitochondrial calcium. *Nat. Rev. Mol. Cell Biol.* **19**, 713–730 (2018).